Experiments on convective heat transfer of air-flows at low Reynolds Number through wavy and grooved channels

A. Muzzio, A. Niro

Dipartimento di Energetica, Politecnico di Milano, piazza Leonardo da Vinci 32, I-20133 Milano, Italy

Abstract

This paper presents experimental data on heat transfer coefficients and pressure drops of air-flows at Reynolds number ranging between 500 and 7000 inside a wavy channel and two grooved channels. Data for a plain channel are also reported for comparison. All channels have a rectangular cross-section with ribs or grooves perpendicular to the streamwise direction; the channel height is 15 or 18 mm. The wavy channel is characterized by triangular cross-section ribs spaced by flat strips, which alternate staggered on the lower and upper walls; the other two channels have grooves only on the lower wall with an aspect ratio of 1:1 and 2:1, respectively. Local heat transfer characteristics are investigated by non-intrusive measurements of velocity and temperature fields by means of LDV and holographic interferometry; data on average coefficients and pressure drops are also reported. Data for Re≤2000 are compared to the results of direct numerical simulations obtained by means of a CFD commercial code. For the wavy channel, the heat transfer enhancement is quite small (20%) within laminar regime while it becomes a quickly increasing function of Re for values greater than 1300; however, pressure drops also start to steeply increase. The grooved channels are characterized by a poor enhancement (30%) but without significant penalization in pressure drops.

1. Introduction

Air-flows inside narrow rectangular channels are frequently encountered in compact heat exchangers with extended surfaces and in microelectronic packages. Due to the small passages and relatively low air velocity, flow is laminar or weakly turbulent and, therefore, convective coefficient is low. When augmented heat transfer is desired, specially configured extended surfaces, such as offset strip, louvered, perforated, and wavy, are largely employed because they increase convective coefficient from 50 to 150% while keeping cost-effectiveness and reliability. The heat transfer augmentation is obtained mainly by altering the duct fluid-dynamic rather than by increasing surface. Many enhancement mechanisms have been explored; however, the most frequently used are periodic deflection of streamlines, periodic interruptions of the boundary layer growth and flow destabilization. Furthermore, corrugations also promote turbulence development, since their size is close to that of the structures to be excited (the lower the Reynolds number, the larger these structures). As the shape of these specially configured fins depends on the enhancement mechanisms employed, there is a large variety of geometries and, consequently, a large number of studies in the open literature. For instance, Webb (1994) reports more than 35 papers and almost as many are cited by Fiebig (1996). For offset strip fin geometry, correlations for predicting the Colburn and friction factors were proposed by Kays (1972), Joshi and Webb (1987), and Wieting (1975); similar correlations were developed by Davenport (1984) for louvered fin geometry. Finally, wavy fin geometry is also the subject of some interesting studies, such as those by Goldstein and Sparrow (1977) and Ali and Ramadhyani (1992), but there are not quite general correlations for this geometry because of a rather lacking data base. For these motivations, we are currently performing an experimental and numerical investigation on flows through channels with wavy or grooved walls.

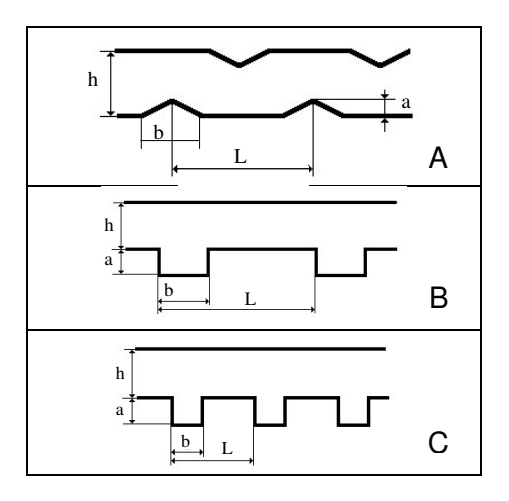
This paper reports on heat transfer characteristics of air-flows inside a wavy channel and two grooved channels at low Reynolds number encompassing laminar, transitional and weakly turbulent regime. Data for a plain channel are also reported for comparison. The wavy channel is characterized by triangular cross-section ribs alternated by flat strips; the rib apex on one of walls coincides with the middle of the flat strip on the other wall. The other two channels have rectangular cross-section grooves only on the lower wall with an aspect ratio of 1:1 and 2:1, respectively. The wavy channel should induce a periodic deflection of the streamlines, whereas the geometric characteristics of the grooved channels should be favorable to a flow destabilization by likewise traveling waves; specifically, the channel with 2:1 aspect ratio is equal to that numerically studied by Ghaddar et al. (1986). They found that at a Reynolds number greater than a critical value (lower than one marking the

laminar to turbulent transition) large-amplitude self-sustained flow oscillations set in which closely resembled Tolmienn-Schlichting channel waves. Local heat transfer characteristics are experimentally investigated for Re≤4000 by non-intrusive measurements of velocity and temperature fields by means of LDV and holographic interferometry, respectively. Experimental data on average heat transfer coefficient and pressure drop for Reynolds number up to 7000 are also reported. Finally, data for Re≤2000 are compared to the results of direct numerical simulations obtained by means of a CFD commercial code.

2. Experiments

The experimental setup consists of two independent circuits, namely, the air circuit containing the test section and the heating water circuit. Through an opening with rounded surfaces, room air flows into an entry section, that is a rectangular duct with the same transverse dimensions as the test section and with a length of 1 m (30 times the hydraulic diameter); the walls of this section are not heated. At the end of this duct, fully developed flow condition is reached and air enters the test section. This is a 200 mm wide, 800 mm long channel with a height of 15 or 18 mm. The side walls of the test section are glass windows to permit optical access to its inside; the lower and upper walls are manifactured with aluminum blocks mounted side by side and strongly tightened to the heating water channel (water flows with a high mass flow rate in the opposite direction of air). To check temperature is uniform over the heated walls, six thermocouples are embedded in the lower wall and two in the upper one, with the tip displaced 0.5 mm from the surface in contact with air. Downstream the test section, there are a 0.5 m long exit section, a filter, three float-type flow-meters, a metering valve and a blower operating in suction mode. The exhausted air is discharged outside the laboratory. The heating circuit is mainly composed by a heat bath with a high precision controller, which provide constant temperature water to the test.

Air temperature is measured at the entrance of the test section, downstream the filter, and upstream and downstream the flow-meters. To obtain average heat transfer coefficient over the channel, air bulk temperature at the outlet of the test section is also measured; in this case, the exit section is equipped with two rows of turbolizers and with a convergent channel that conveys air flow through a narrow duct (1 cm in width) filled with a tangle of metallic fine wires where two thermocouples are embedded. Flow velocity profile measurements are obtained for five different traverses, 5-10 mm apart each other, by the LDV technique using a TSI system which includes a fiberoptic probe and the IFA750 signal processor; the velocity profile consists of 15-20 points and each measurement is the average of five readings based on a 1024 data sample. The temperature field is measured by means of real time holographic interferometry. A two-beam interferometer is used with a He-Ne laser, 35 mW power as light source. The reference state of the air flow, corresponding to the experimental setup at the room temperature, is first recorded on a photographic plate; the plate is then processed and accurately repositioned into its original location by means of electrostrictive micro-positioners. Finally, the reference state is reconstructed by illuminating the plate, while the convective heat transfer phenomena to be investigated occur, and this results in a real time interference. Principles and methods of the holographic interferometry are reported in Vest (1979). Interferograms are electronically recorded by a CCD camera with 384x512 pixels and transmitted into a PC with a 8-bit frame grabber. The evaluation of interferometric images consists in reconstructing the phase-difference distribution from the light-intensity distribution, and it has been performed using the classic method based on maximum/minimum fringe location (Hauf and Grigull, 1970) and, in some cases, we started to adopt a phase-shifting method (for a given state, more interferograms are recorded while shifting the phase of one of the interferometer beams of a time-constant amount). This method is characterized by higher sensitivity, since it can resolve phase-differences up to one hundredth of the source wave length, but it requires a more complex experimental setup and advanced numerical techniques for evaluating interferograms. Once the phase-difference distribution has been evaluated, the two-dimensional temperature field is determined by means of the ideal interferometry equation. Temperature profiles are obtained for 20-30 traverses equally spaced along a corrugation pitch, included the traverses where the velocity profiles have been measured so that the bulk temperature can be also evaluated. Eventually, the local Nusselt number is calculated as $Nu=[-D_h(\partial T/\partial n)_w/\theta]$ where $(\partial T/\partial n)_w$ is the temperature normal derivative evaluated on the wall, D_h the hydraulic diameter, $\theta = (T_w - T_b)$ the wall to air bulk temperature difference; the average Nusselt number over the entire heated length L is evaluated as $Nu_L = [0.25 (D_h/L) \text{ Re Pr } ln(\theta_i/\theta_o)]$ where θ_i and θ_o are the wall to air bulk temperature difference at the entrance and the exit of the channel, respectively. Pressure drops are measured by means of a differential



	Channel	A	В	С
Parameter				
h	[mm]	15	18	15
a	[mm]	3	10	10
b	[mm]	20	20	10
L	[mm]	30	60	30
Width	[mm]	200	200	200
Hydraulic diameter	[mm]	27.9	32.7	27.9
Heigth to width ratio		0.075	0.090	0.075
Ribs/grooves number	·	25	13	26

Figure 1. Channel geometry.

Table I. Main geometrical parameters.

liquid micro-manometer through two probes plugged into the channel; the probes consist of 8-mm o.d. tube with two pairs of 0.1-mm pressure taps.

3. Results and Discussion

The geometry of the channels investigated in this paper is schematically showed in Fig. 1, whereas Tab. I lists their main characteristic parameters. The presentation of results will begin with the local Nusselt number in the periodic fully developed regime. Fig. 2 reports the streamwise distribution of the local Nusselt number along both the lower and upper wall of channel A. Data are referred to axial locations around the seventh corrugation of the lower wall and the graph relevant to the upper wall has been translated downstream of half a pitch to allow for a better comparison. Also shown in this figure are the numerical values of the Nusselt number computed by means of a commercial finite element code and the limiting value of the Nusselt number for fully developed laminar flow in a rectangular duct with two isothermal and two adiabatic walls, which is equal to 6.68. This latter value was obtained by interpolating the data reported by Shah and London (1978). Inspection of the data shows that the local Nusselt number increases along the upstream-facing facet and changes abruptly at the peak of the corrugation where it exhibits a maximum with values four-five times as high as in the plain channel. At the valleys, owing to the presence of a large separation bubble, the Nusselt number is well below the overall average for the corrugated wall and even lower than that one pertaining to the straight duct. The difference in Nusselt numbers between peak and valley increases with increasing Reynolds number. However, the per-module Nusselt number only slightly exceeds the corresponding value for the straight duct in this range of Reynolds numbers, as will be shown later on. Furthermore, the establishment of periodic fully developed regime can be inferred from the good matching of the experimental Nusselt number at the ends of a cycle of corrugation.

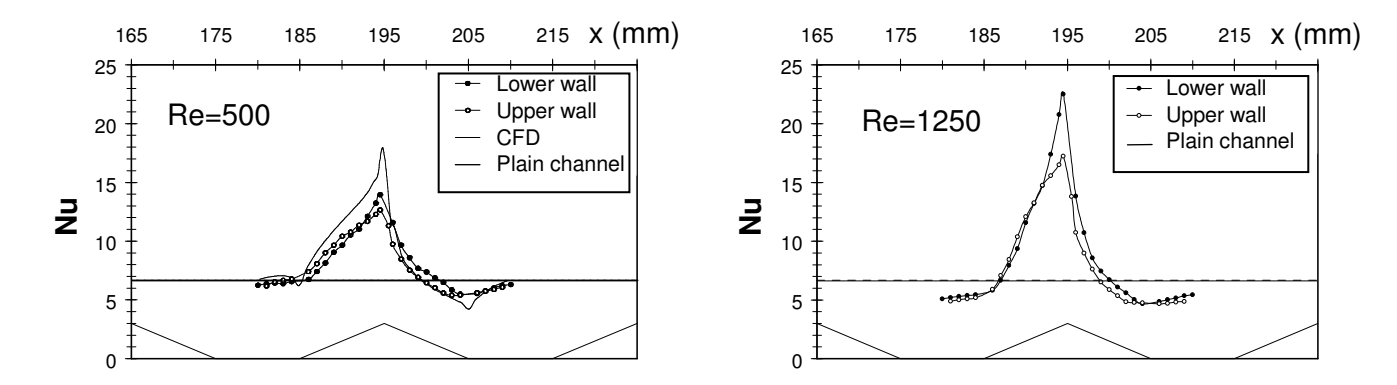


Figure 2. Streamwise distribution of local Nusselt number around the seventh lower rib inside the channel A.

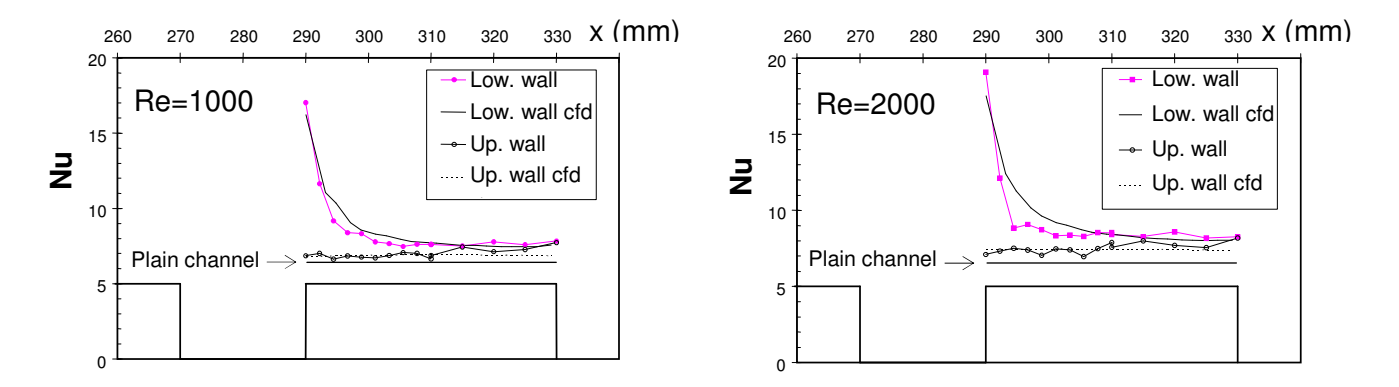


Figure 3. Streamwise distribution of local Nusselt number around the sixth groove inside the channel B.

The streamwise distributions of the local Nusselt number along the upper and lower wall of channel B are presented in Fig. 3. Data points span the wall region situated between the sixth and seventh groove and correspond to Reynolds numbers of 1000 and 2000. The heat transfer at the bottom of the groove was apparently very low. However, the relevant results are here omitted as the interferograms obtained with infinite field fringe alignment could not be processed with sufficient accuracy in this region. An overall review of the results along the lower wall indicate a trend that is to some extent similar to the distribution of heat transfer coefficients over a flat plate in parallel flow. As seen, the local Nusselt number drops off immediately downstream of the reattachment edge, where the redevelopment of the boundary layer takes place, and then gradually reaches a pseudo-asymptotic value which exceeds that one for the plain channel. The height of the reattachment peak increases with increasing Reynolds number as well as the pseudo-asymptotic value though to a much lesser extent. With regard to the local Nusselt number distribution along the upper wall, it can be seen that it keeps practically constant and almost equal to the plain channel value. Therefore, it can be inferred that the presence of the grooves does not affect the heat transfer on the upper wall. Also shown in this figure are the numerical results which show a good agreement with the experimental ones. Finally, the per-module (including the groove) Nusselt number for this channel slightly exceeds the plain channel value as the high Nusselt numbers induced by the periodic formation of the boundary layers at the interrupted surfaces level off rapidly and are counteracted by the poor heat transfer in the cavity. Based on this consideration, a different channel, referred as channel C, was tested. Its configuration was obtained from the previous one by halving the width both of groove and of flat-strip while keeping constant the groove depth. As a consequence, channel C has the same area of the flat-strips as channel B and is characterized by square cavities. The streamwise distributions of local Nusselt number along the upper and lower wall of this channel are shown in Fig. 4. The data in this figure pertain to the region around the thirteenth cavity and correspond to Reynolds numbers of 1000 and 1500. From the inspection of the figure we can recognize a trend

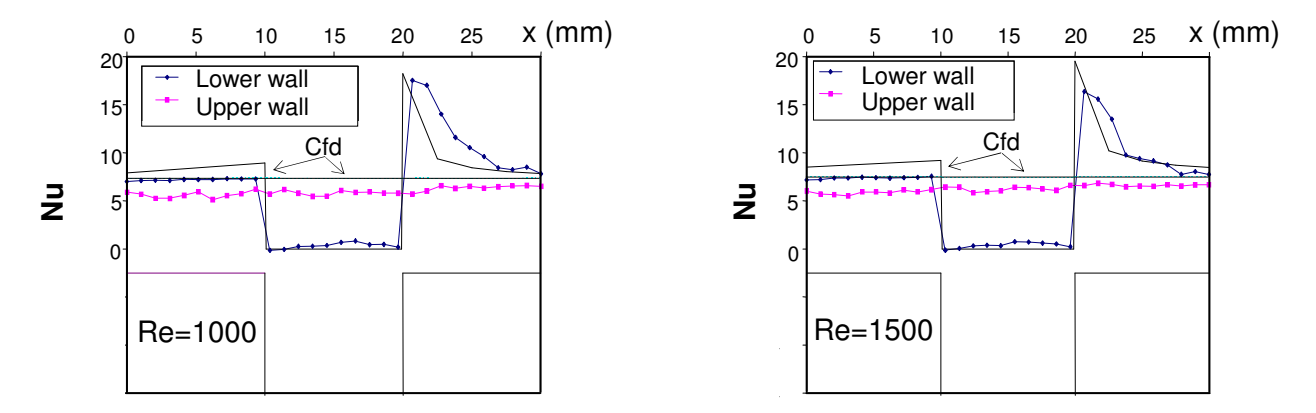


Figure 4. Streamwise distribution of local Nusselt number around the sixth groove inside the channel C.

similar to that for channel B. As expected, the length of the flat-plate segment at constant Nusselt number is shortened and consequently the average Nusselt number along the flat strip exceeds that one of channel B by about 11%. However, the per-module average Nusselt number only exceeds by about 5% that one of channel B owing to the weight of cavity and to the upper wall. It is worth noticing that in this case the use of phase-shifting holographic interferometry permitted the measurement of heat transfer coefficients also at the cavity bottom. Consideration will now be given to the average transfer coefficients and to the pressure drop over the whole channel. Owing to the significantly simpler data acquisition requirements, a substantially larger number of runs were able to be made to obtain average heat transfer coefficients than were performed for the local coefficient study. The Reynolds number range for the average coefficients extended from about 500 to 7000 for channel A, to 4000 for channel B and to 5000 for channel C. The results thus obtained are presented in Fig. 5 in terms of the average Nusselt number and in Fig. 6 in terms of apparent Darcy friction factor. In addition to the present data, the figures contain information relevant to the rectangular duct from the literature. It was included on the plots for comparison. The solid line in Fig. 5 depicts the prediction of the correlation due to Hausen for Re>2300 and the fully developed Nusselt number in laminar flow for Re<2000 (Shah and London, 1978). The dots on Fig. 6 correspond to measurements of friction factor performed inside a plain channel with a height of 15 mm. From the overall inspection of Figs. 5 and 6, it is seen that channels B and C exhibit qualitatively similar trends that differ markedly from channel's A. As for the wavy channel A, it appears that in the range of Reynolds numbers up to about 1250 the Nusselt number is essentially constant and the deviation of the data from the limiting value of Nusselt number for laminar flow in the plain channel is only 20 percent. Therefore, it can be inferred that wall corrugation significantly alters the distribution of the local Nusselt number without affecting its average value to a large extent. This can be considered a surprising outcome, inasmuch as larger differences would have been expected on the basis of geometrical and flow field differences between the two types of channel. However, similar findings have been reported by Goldstein and Sparrow (1977) and by Ali and Ramadhyani (1992) in their studies of corrugated wall channels. Above Re=1250 the data for the wavy channel begin to rise steeply with increasing Re, before attaining a more gradual slope (comparable to that of the Hausen correlation) at around Re=3000. The onset of this rapid rise in Nusselt number could be indicative of the flow becoming transitional between the steady laminar and turbulent regimes. In comparison with the plain channel results, substantial heat transfer enhancement is achieved in the wavy channel for Re>1250. For instance, a heat transfer enhancement factor of nearly four is attained at Re=7000. This indicates that wall corrugation can serve as effective augmentation devices for turbulent flow at low Reynolds number. However, the heat transfer augmentation is largely penalised by the accompanying increase of the apparent friction factor that exceeds the plain channel value by a factor of 1.5÷3 in laminar flow regime and by a factor of even ten in turbulent flow regime. Turning next to channels B and C, it may be noted that the average Nusselt number curves are practically identical for the two grooved channels within the range of Reynolds numbers up to about 2300. This result is in agreement with

the local heat transfer study which showed that in the laminar-range the per-module average Nusselt numbers for channel C were only moderately larger than those for channel B. Contrary to channel A, the Nusselt number gra-

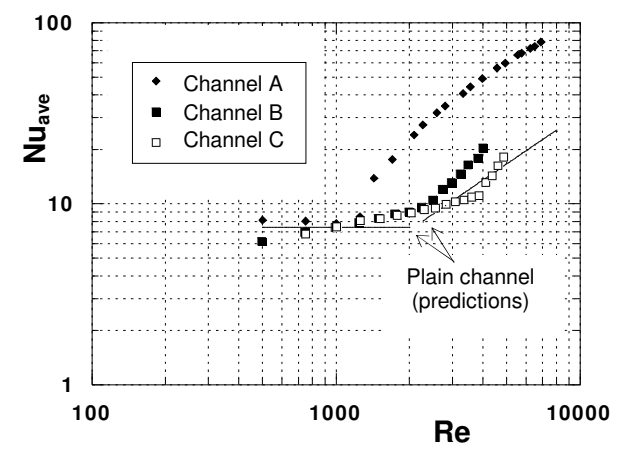


Figure 5. Average Nusselt number vs. Reynolds number.

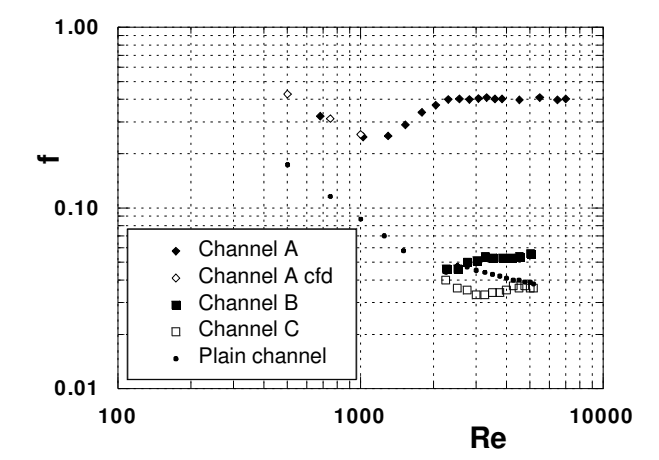


Figure 6. Friction factor vs. Reynolds number.

dually increases with Reynolds number in the range of Reynolds numbers up to about 2300, where a leastsquares correlation of the data yields an exponent on the Reynolds number of about 0.33. The heat transfer enhancement with respect to the plain channel, vanishes at Re=500 but goes up to about 30% at Re=2300. Then, somewhere between Re=2300 and 2500, there is a change of slope for channel B so that, thereafter, the Nusselt number increases more rapidly. In fact, a least-squares correlation of the data yields an exponent on the Reynolds number of about 1.33 for Re>2500, where a substantial heat transfer enhancement is achieved in comparison with the rectangular plain channel. In accordance with the results of the flow visualisation studies, the onset of this more rapid rise in Nusselt number could be attributed to the transition from laminar to turbulent flow. Instead, the change of slope for channel C is observed to occur at a Reynolds number of about 4000, thus confirming the results of the flow visualisation about the persistence of the steady laminar flow in this channel. Beyond the transition, the data for channel C begin to rise steeply with a slope comparable to that of channel B. Finally, the apparent friction factor for channel B is nearly equal to that for the straight rectangular channel in the range of Reynolds number up to about 2500. At higher Reynolds numbers, increased energy dissipation due to the onset of transitional flow, leads to sizable deviations from the plain channel; for instance, at Re=5000, the relative increase in the apparent friction factor is more than 40 percent. As for channel C, it is interesting to note that the delay in the onset of turbulent flow results in apparent friction factors lower or at the most equal to those for the straight rectangular duct. For instance, at Re=3000 where the maximum deviation occurs, it is found that the relative decrease is about 30 percent.

4. Conclusions

Experimental data on local and average convective coefficient and on pressure drop inside a wavy channel (A) and two grooved channels (B and C) have been reported. For channel A, the heat transfer enhancement with respect to a plain channel is only 20% within laminar regime while the average Nu becomes a quickly increasing function of Re for values greater than 1300; however, pressure drops also start to steeply increase. The grooved channels exhibit trends of average Nu markedly different from channel's A, but qualitatively similar between them unless the laminar to turbulent transition occurs at higher Re inside the channel C. Finally, the heat transfer enhancement is rather poor (30%) but they are not affected by a significant penalization in pressure drop.

Acknowledgments

This work is supported by MURST (the Italian Ministry for the University and for the Scientific and Technical Research) via PRIN 1999 grants.

References

Ali, M.M., Ramadhyani, S., Experiments on convective heat transfer in corrugated channels, Experimental Heat Transfer, Vol. 5, pp. 175-193, 1992.

Davenport, C.J., Correlations for heat transfer and flow friction characteristics of louvered fin, Heat transfer-Seattle 1983, AIChE Symp. Ser., No. 225, Vol. 79, pp. 19-27, 1984.

Fiebig, M., Vortices: tools to influence heat transfer. Recent developments, Proc. 2nd European Thermal Sciences and 14th UIT National Heat Transfer Conference, vol. 1 pp. 41-56, Rome, June 1996.

Ghaddar, N.K., Korczak, K.Z., Mikic, B.B., Patera, T., Numerical investigation of incompressible flow in grooved channels. Part 1. Stability and self-sustained oscillations. J. Fluid Mech., Vol. 163, pp. 99-127 (1986).

Goldstein, L.J., Sparrow, E.M., Heat/mass transfer characteristics for flow in a corrugated wall channel, J. Heat Transfer, Vol. 99, pp. 187-195, 1977.

Hauf, W., Grigull, U., Optical methods in heat transfer, in Advances in Heat Transfer, Vol. 6, p. 133, Academic Press, 1970. Joshi, H.M., Webb, R.L., Prediction of heat transfer and friction in the offset strip fin array, Int. Journal of Heat and Mass Transfer, Vol. 30, No. 1, pp. 69-84, 1987.

Kays, W.M., Compact Heat Exchangers, AGARD Lecture Ser. No. 57 on Heat Exchangers, ed. Ginoux, AGARD-LS-57-72, Jan. 1972.

Shah, R.K., London, A.L., Laminar flow forced convection in ducts, Academic Press, 1978.

Vest, C.M., Holographic interferometry, John Wiley & Sons, 1979.

Webb, R.L., Principles of Enhanced Heat Transfer, John Wiley & Sons, cap. 9, pp. 228-284, 1994.

Wieting, A.R., Empirical correlations for heat transfer and flow friction characteristics of rectangular offset fin heat exchangers, J. Heat Transfer, Vol. 97, pp. 488-490, 1975.